

A Characterization of Cold Pools in the West African Sahel

M. PROVOD

School of Earth and Environment, University of Leeds, Leeds, United Kingdom

J. H. MARSHAM

Water @ Leeds, University of Leeds, Leeds, United Kingdom

D. J. PARKER

School of Earth and Environment, University of Leeds, Leeds, United Kingdom

C. E. BIRCH

Met Office @ Leeds, Leeds, United Kingdom

(Manuscript received 17 January 2015, in final form 9 July 2015)

ABSTRACT

Cold pools are integral components of squall-line mesoscale convective systems and the West African monsoon, but are poorly represented in operational global models. Observations of 38 cold pools made at Niamey, Niger, during the 2006 African Monsoon Multidisciplinary Analysis (AMMA) campaign (1 June–30 September 2006), are used to generate a seasonal characterization of cold pool properties by quantifying related changes in surface meteorological variables. Cold pools were associated with temperature decreases of 2°–14°C, pressure increases of 0–8 hPa, and wind gusts of 3–22 m s⁻¹. Comparison with published values of similar variables from the U.S. Great Plains showed comparable differences. The leading part of most cold pools had decreased water vapor mixing ratios compared to the environment, with moister air, likely related to precipitation, approximately 30 min behind the gust front. A novel diagnostic used to quantify how consistent observed cold pool temperatures are with saturated or unsaturated descent from midlevels [fractional evaporational energy deficit (FEED)] shows that early season cold pools are consistent with less saturated descents. Early season cold pools were relatively colder, windier, and wetter, consistent with drier midlevels, although this was only statistically significant for the change in moisture. Late season cold pools tended to decrease equivalent potential temperature from the pre-cold pool value, whereas earlier in the season changes were smaller, with more increases. The role of cold pools may therefore change through the season, with early season cold pools more able to feed subsequent convection.

1. Introduction

Mesoscale convective systems (MCSs) form an integral part of the West African monsoon (Flamant et al. 2007; Marsham et al. 2013a) and account for more than 80% of the annual rainfall in most of the Sahel (Mathon

et al. 2002; Dhonneur 1973). Cold pools produced by MCSs are important for a number of reasons: they are a key mechanism for maintenance of the MCSs, and for secondary initiation of new cumulonimbus systems; they transport substantial amounts of cold air northward, cooling and moistening the Saharan heat low by advection (Marsham et al. 2013a; Garcia-Carreras et al. 2013); they are responsible for around 50% of summertime dust uplift in the Sahel and Sahara (Marsham et al. 2008, 2011b; Heinold et al. 2013; Marsham et al. 2013b);

 Denotes Open Access content.

Corresponding author address: M. Provod, School of Earth and Environment, University of Leeds, Clobbery St., Leeds LS2 9JT, United Kingdom.
E-mail: eempr@leeds.ac.uk



This article is licensed under a [Creative Commons Attribution 4.0 license](https://creativecommons.org/licenses/by/4.0/).

DOI: 10.1175/MWR-D-15-0023.1

and they are associated with intense rain and strong winds.

In the summer, seasonally increasing southwesterly monsoon winds advect moist high equivalent potential temperature (θ_e) low-level air into the Sahel, which undercuts the dry midlevel Saharan air layer (SAL; Parker et al. 2005). The SAL is characterized by almost dry adiabatic lapse rates, which together with the low-level moisture results in large quantities of convective available potential energy (CAPE). There is, however, high convective inhibition (CIN), which together with midtropospheric dry air needs to be overcome for deep convection to be initiated and sustained.

Localized triggering initially creates discrete small-scale convective storms (Dione et al. 2014) that can, under certain conditions, grow upscale to form an MCS, often in the form of a propagating squall line (Hamilton et al. 1945; Aspliden 1976; Fortune 1980; Chong et al. 1987; Lebel and LeBarbe 1997; Lebel et al. 1997; Futyant and Del Genio 2007; Chong 2010; Lothon et al. 2011; Birch et al. 2013). Because of the presence of midtropospheric dry air masses in the Sahel, latent cooling caused by evaporation, melting, or sublimation of hydrometeors is supportive of the formation of a cooler than environmental downdraft (Redelsperger and Lafore 1988). This cooler air then reaches the surface and spreads out as a density current (i.e., the cold pool) (Charba 1974; Mueller and Carbone 1987). Together with the ambient wind shear, the cold pool helps to lift surrounding air parcels (e.g., Dione et al. 2014) and create new cells, organizing the MCS (Roca et al. 2005). Therefore, cold pools play an important role in organizing deep moist convection and are an integral part of MCSs (Thorpe et al. 1982; Rotunno et al. 1988; Weisman et al. 1988; Fovell and Ogura 1989; Szeto and Cho 1994a, b; Trier et al. 1997; Parker and Johnson 2004a,b).

Perhaps the largest observational study of cold pool properties to date is based in the United States over Oklahoma and was performed by Engerer et al. (2008, hereafter ESC08). Their study investigated 39 squall-line MCSs by using data from 110 mesonet stations across the state of Oklahoma and they obtained 1389 time series of cold pool-related variables. The cold pool quantities studied by ESC08 were decreases in potential and equivalent potential temperature, pressure rises, changes in wind direction, and maximum wind gusts. The focus of their study was on the evolution of cold pool properties during various life cycles of MCSs as well as comparison of the observed cold pool characteristics with idealized model simulations. Given that this study was based in the United States, it is of interest to assess whether the particular conditions of MCSs in West Africa result in comparable distributions of cold pool properties. As far as the authors

are aware, there are several case studies of West African MCSs (e.g., Chong 2010; McGraw-Herdeg 2010), but to date there is no general characterization of surface cold pool properties.

This paper studies observed properties of West African cold pools produced by organized MCSs, mostly squall lines, and compares them to results obtained in Oklahoma by ESC08. One goal of this paper is to provide observational results for future studies to better evaluate cold pools in models. The monsoon season is split into three subperiods to enable evaluation of seasonal evolution of MCS-related cold pool properties. Section 2 describes the observational datasets and the analysis method. Section 3a focuses on thermodynamic properties such as pressure and temperature and their seasonal variations. Section 3b studies cold pool winds. Section 4 summarizes the results and discusses their implications.

2. Data and methods

a. Data

The African Monsoon Multidisciplinary Analysis Special Observing Period (AMMA SOP) took place in 2006. Documentation of MCSs was one of the key components of AMMA and the data obtained during AMMA currently provide the most detailed and complete dataset for moist convection in West Africa (Redelsperger et al. 2006).

The Massachusetts Institute of Technology (MIT) C-Band Doppler radar was deployed near Niamey, Niger (13.5°N, 2.2°E), during AMMA. Scans were recorded at 10-min intervals during the AMMA radar observing period (AMMA ROP), which ran from 5 July 2006 until 27 September 2006. For the purpose of this study we used 360° long-range (250 km) surveys at 0.7° elevation in addition to Meteosat infrared satellite images.

The Atmospheric Radiation Measurement (ARM) Climate Research mobile facility was deployed at Niamey airport. Surface meteorology data obtained from this station were used in this study (Holdridge et al. 2013a). The surface data consist of pressure, temperature, relative humidity, 10-m winds, and rainfall intensity. For the purpose of this study, these data were used to calculate surface equivalent potential temperature and water vapor mixing ratio (WVMR). These were available in minute-averaged intervals for the whole AMMA SOP.

Radiosondes were released daily from Niamey airport approximately 30 min before 0000, 0600, 1200, and 1800 UTC (Holdridge et al. 2013b). Some days had additional radiosonde releases approximately 30 min before 0300, 0900, 1500, and 2100 UTC. Local time is identical to UTC time (with solar noon at 1157 UTC 15

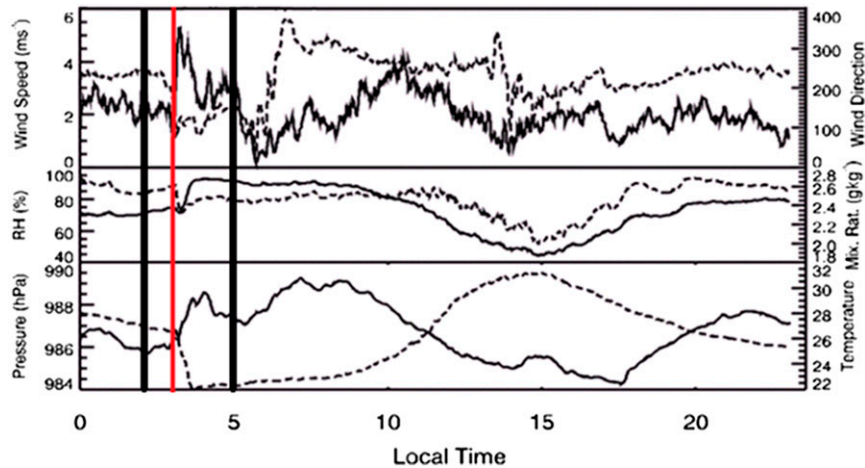


FIG. 1. An example of an observed daily time series as obtained by the surface station at Niamey airport. This time series is for 11 Aug 2006, when a cold pool crossing was identified at 0315 local time (LT) (denoted by the vertical red line). Black lines denote the borders of the time windows used for the analysis. Solid lines correspond to left-hand axis and dashed lines correspond to right-hand axes. Data were recorded every second and averaged at minute intervals.

July 2006). There were, however, days when radiosonde ascents were missing or delayed.

b. Method

The study period spanned from 1 June to 30 September 2006. A very similar approach to ESC08 has been applied to allow comparison between West African MCS cold pools and ESC08's results from the United States. ESC08 subjectively identified cold pool crossing times and then objectively quantified changes in surface station variables from the 30 min preceding the cold pool crossing to the 2 h subsequent to the crossing. The 30-min time window used to detect prestorm maxima and minima in surface variables used by ESC08 was not always long enough to capture these in Niamey, mainly in cases of pressure as the prestorm minimum was on average 52 min ahead of the cold pool. Therefore, in this study, the prestorm time window was extended to 1 h before the cold pool arrival time.

Time series of surface station data for a sample cold pool, observed on 11 August 2006 at Niamey Airport, are shown in Fig. 1. Cold pool crossings are associated with a sudden change in wind direction (ESC08; Fujita 1963) and as in ESC08 the wind direction change was considered to be the main factor in the identification of crossing times (e.g., Fig. 1). Times of sudden wind direction changes were subjectively identified and counted as potential cold pools. In order for the wind direction change to be sudden, it must have happened within 5 min and been of at least a 30° magnitude. Because a wind direction change may, however, be associated with

features other than cold pools [e.g., dust devils (Tratt et al. 2003), or gravity waves (Cram et al. 1992; Birch et al. 2013)], the other surface variables were also considered as specified below.

The change in wind direction must have occurred within 30 min of a wind gust and changes in temperature and pressure to be counted as cold pool related. The magnitude of the gust must have been at least 1.5 times greater than the mean wind speed in the 30 min before the gust and temperature must have dropped by at least 1°C (e.g., Fig. 1). It is not likely, but possible, that something other than an MCS cold pool in the Sahel would cause these changes in pressure, temperature, and wind. Because of this limitation of using surface data only, all the identified cold pools were verified by considering images from the MIT radar or satellite (outside of the ROP). This verification has been done subjectively based on inspection of radar/satellite images to see whether an MCS has been present in the vicinity of Niamey at the time of the cold pool passage.

Following the approach of ESC08, the cold pool-related changes in surface variables were calculated for 1) an increase in pressure (the maximum after the cold pool minus the minimum before), and 2) a decrease in temperature (maximum before minus the minimum after). For 3) equivalent potential temperature (θ_e), cold pools could give an increase or a decrease, and often short-lived fluctuations complicated any method based on minima and maxima; therefore, unlike ESC08, changes in mean from the period spanning 1 h before the cold pool crossing time to the period spanning 2 h after

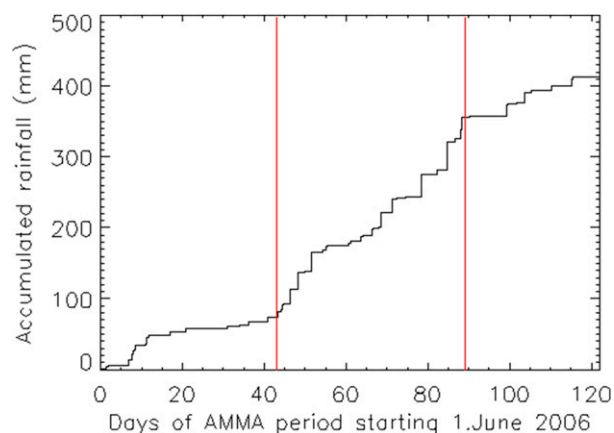


FIG. 2. Total accumulated rainfall from Niamey ARM surface station data. Red lines separate three seasonal periods used in this study: “premonsoon” (1 Jun–12 Jul 2006), “monsoon” (13 Jul–27 Aug 2006), and “retreat” (27 Aug–30 Sep 2006).

the crossing were calculated. In addition, unlike ESC08, 4) a change in WVMR and 5) an increase in mean wind speed were also calculated. For WVMR, the mean value in the hour before the cold pool was subtracted from the minimum value in the 2 h after (so positive values show moistening). The minimum after the passage was used rather than the maximum as there was often a sharp minimum just following a cold pool passage, that was often followed by an increase that reached greater than pre-cold pool magnitudes within the 2 h, but which was likely not primarily related to the cold pool crossing (e.g., Fig. 1). The mean value in the 1 hour before the cold pool was used rather than a maximum in order to take into account the sometimes sharp fluctuations in WVMR that were likely related to turbulence and mixing. In addition, the maximum wind gust associated with the cold pool was obtained by taking the maximum wind speed in the 2 h after the cold pool crossing (as in ESC08).

For a majority of the studied cold pools, the cold pool-related changes in surface variables were coincident or nearly coincident. There were, however, several cases where this was not the case and, hence, it was difficult to define the cold pool crossing time. This was most frequent in case of wind direction changes, where in several cases there were multiple wind direction changes of more than 30° within ~ 2 h of a wind gust, but none coincided with the actual wind gust. These were likely related to waves propagating faster than the cold pool from the parent storm. In such cases either the time of the closest wind direction change to the gust or the time of the actual gust was taken as the crossing time, based on whichever was closest to the temperature drop. Because of this there is clearly uncertainty in the cold pool

crossing times, but ESC08 show the objectively determined changes are generally robust to the precise crossing time used.

Using the radar and Meteosat imagery, the storms generating the cold pools were separated subjectively into isolated storms and larger organized convective systems (MCSs; spanning at least 100 km as defined by the American Meteorological Society 2015). The main difference between the methods of ESC08 and this study is that MCS life cycle stage differentiation was not used because there was one radar available in the Sahel, which is not enough information to decide on the life cycle stage as it covers only a fraction of the MCSs life cycle. Instead, data were separated by subperiods.

It was hypothesized that cold pool intensity would depend on midlevel dryness. Therefore, the whole season was divided into three subperiods based on the seasonal evolution of rainfall at Niamey (Fig. 2). We refer to these subperiods as: “premonsoon” (1 June–12 July 2006), “monsoon” (13 July–27 August 2006), and “retreat” (27 August–30 September 2006), although they are not based on any formal definition of monsoon onset. The subperiod boundaries were set based on subjectively identified changes of slope in the observed time series of accumulated rainfall (clearest for premonsoon to monsoon). Out of the 38 cold pools used in this study, 22 occurred in the monsoon subperiod with 8 in the premonsoon and 8 in the retreat subperiods.

3. Results and discussion

During the study period, 42 cold pools were detected. Of these, 33 were squall-line MCSs (having a continuous line being at least 100 km in length and having reflectivity of at least 35 dBZ along at least 50% of its length), 4 were non-squall-line MCSs, one was a propagating cold pool from a freshly dissipated MCS (seen in satellite imagery but out of radar range), and 4 were from local non-MCS convection (there were many isolated convective storms in the range of the MIT radar, but their cold pools rarely crossed Niamey). The four cold pools related to the isolated convection gave very limited statistics and since this study focuses on cold pools produced by organized MCSs, data from these four cases were not used in the analysis.

Figure 3 shows composites of surface variables, centered on cold pool crossing time. The “composite cold pool,” (over the entire observation period, black lines), was accompanied by a decrease in temperature of 5.3°C . As expected, the cooling of the cold pool brings a pressure increase, the magnitude of which was 1.9 hPa. The wind maximum related to the cold pool passage

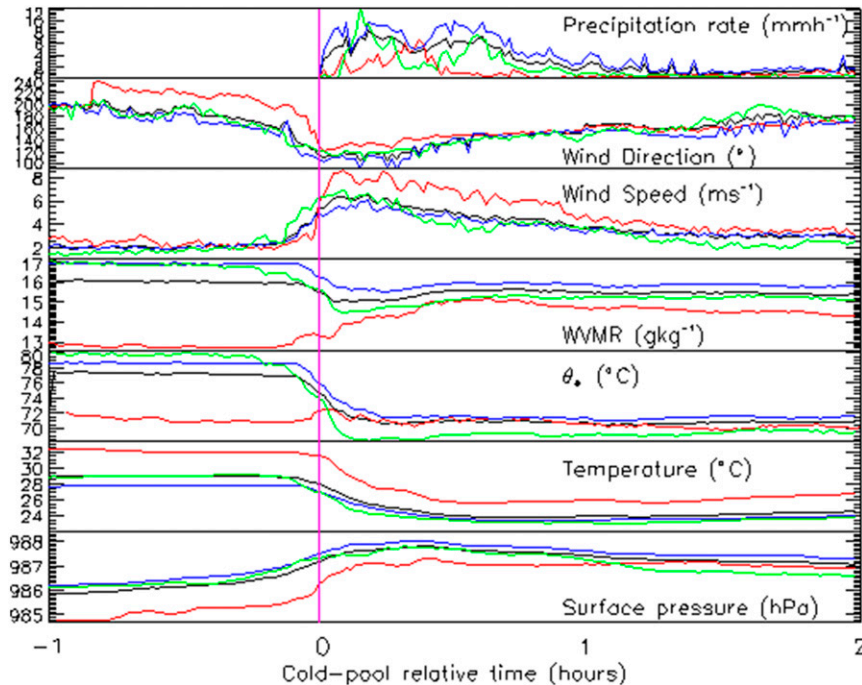


FIG. 3. Composite cold pools are obtained from averaging variables of all cold pools around the crossing time. The black line is for the whole period, red is for the premonsoon period, blue is for the monsoon, and green is for retreat. The vertical pink line shows the cold pool crossing time.

had a magnitude of 6.5 m s^{-1} in the composite, with the wind rotating from approximately 200° to 120° . Rainfall intensity increased rapidly to a maximum about 15 min after the cold pool passage with a second peak approximately 45 min after the passage. The weaker precipitation behind the first peak corresponds to the “weak echo” in the radar observations, between stratiform rain and the main line of convective cells. WVMR decreased after the initial passage and stayed low throughout the first “convective rainfall” maximum. Approximately 30 min after the cold pool passage, there was a small increase of WVMR (accompanied by an increase in relative humidity, not shown). Although only around 0.5 g kg^{-1} this change is approximately twice the standard error in the composite of cold pool changes (not shown) and this temporary decrease followed by an increase was observed in 26 out of 38 cases. The increase was coincident with the second “stratiform” rainfall peak. This drying and moistening coincidence with the rainfall suggests that there may be a descent of dry midlevel air toward the surface occurring during the convective rainfall occurrence, while later evaporation of stratiform rain increases WVMR.

Figure 3 shows that cold pool–related changes are different across the subperiods. Premonsoon cold

pools are associated with greater pressure increases, temperature decreases, less intense and shorter-lived precipitation, and stronger winds. Furthermore, the related changes in equivalent potential temperature and WVMR vary. The statistical significance of these seasonal differences is investigated in later sections. All values given below are means and standard deviations. The composite premonsoon cold pools caused a long-lived WVMR increase of $2.5 \pm 0.8 \text{ g kg}^{-1}$, while during the monsoon and retreat there are long-lived decreases of 1.5 ± 0.2 and $2.7 \pm 0.5 \text{ g kg}^{-1}$, respectively. Equivalent potential temperature changes very little with a premonsoon cold pool passage. In contrast, there is a sharp and long-lived decrease in equivalent potential temperature in the monsoon and retreat subperiods, with the decrease during the retreat being greater than during the monsoon ($11.9^\circ \pm 10^\circ\text{C}$ and $7.8^\circ \pm 4.8^\circ\text{C}$, respectively). The rainfall structure of premonsoon MCSs also appears to be different: the two rainfall peaks are less clear and later stratiform rain makes a smaller contribution to the total.

a. Thermodynamic properties of cold pools

Figure 4 shows bar plots of the normalized frequency distribution of several cold pool properties and their seasonal variations. The bars are normalized to allow

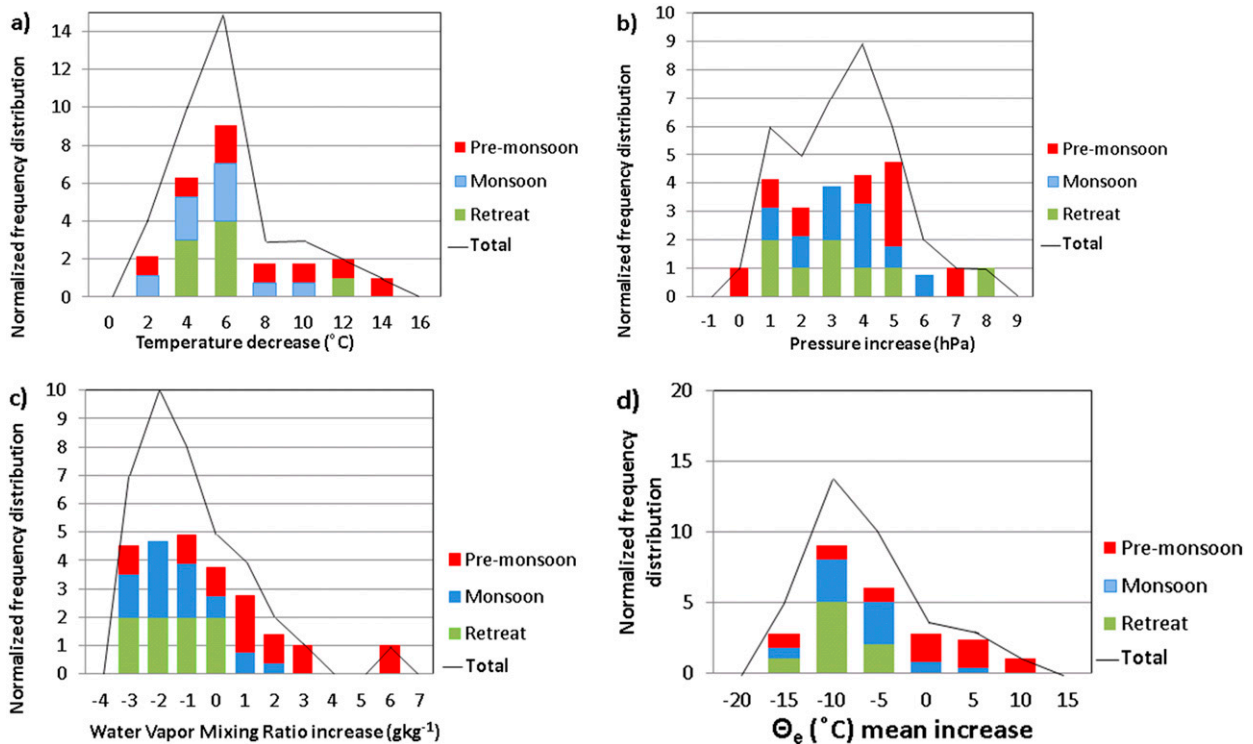


FIG. 4. Changes in specified thermodynamic variables from cold pools: (a) decrease in temperature, (b) increase in pressure, (c) increase in WVMR, and (d) increase in mean θ_e . Coloring represents the subperiods (red: premonsoon, blue: monsoon, green: retreat). Number of events in each season is normalized to allow a comparison between seasons (see text) with the black line showing total (unnormalized) distributions.

comparison between subseasons and account for the different numbers of cold pools identified in the three subperiods. There were 8 events each in premonsoon and retreat and 22 in monsoon; therefore, monsoon was normalized by multiplying the number of events by 8/22 to allow comparison. The black line that shows the frequency distribution over all three subperiods, therefore, only overlies the top of the bar plots when there are no monsoon events in that bin.

A temperature decrease between 1.8 $^{\circ}$ and 13.1 $^{\circ}\text{C}$ was observed for all cold pool passages (Fig. 4a). The whole seasonal distribution is skewed, however, with a broad peak between approximately 3 $^{\circ}$ and 7 $^{\circ}\text{C}$ and only three events of temperature decrease greater than 11 $^{\circ}\text{C}$. The distribution of pressure increase in Fig. 4b is also skewed, ranging from 0.4 to 7.6 hPa, with most events between 1 and 4 hPa. These values are larger than the pressure increase in the cold pool composite in Fig. 3 because the timing of the maximum and minimum pressure relative to the gust front differs between cold pools. This is a limitation of the composite as minima and maxima occur at relatively different times from the time of crossing; partly because cold pools propagate at different speeds and also because for any system the

maxima/minima are located at different positions relative to the gust front.

Figure 4c shows that the majority of cold pools led to a drying, but 10 cold pools (27%) led to an increase in WVMR. The WVMR increase ranged from -3.4 to $+6.1 \text{ g kg}^{-1}$. Most events gave a decrease in mean θ_e with the greatest decrease being -12.6°C , but several events show an increase, with the largest being $+8.7^{\circ}\text{C}$ (Fig. 4d). Bar plots of relative humidity are not shown, but it was found that all cold pools gave increases in RH of magnitudes between 0% and 60%. It was found that the three cold pools with greatest WVMR increases were closest to rain, but no overall relationship could be concluded between the WVMR change and its proximity to rainfall.

There was a tendency toward greater pressure increases and temperature decreases in the premonsoon period when compared to the whole season (mean changes were 3.4 hPa for premonsoon vs 2.9 hPa overall and 7.8 $^{\circ}$ vs 5.9 $^{\circ}\text{C}$ overall). The differences in pressure and temperature changes between subseasons were, however, not statistically significant at the 90% level. Humidity changes from cold pools also varied across the subperiods, with WVMR tending to increase in

premonsoon, but tending to decrease in the rest of the season (means of $+1.1 \text{ g kg}^{-1}$ for premonsoon vs -0.6 g kg^{-1} overall). Mean equivalent potential temperature both increased and decreased in the premonsoon, but nearly always decreased in the remainder of the observation period (mean changes of -2.2° vs -9.6°C). The seasonal differences in changes equivalent potential temperature and WVMR were significant at the 90% level. This premonsoon difference is consistent with drier midlevels during the premonsoon period that promote more evaporation (or sublimation) and hence greater associated moistening, cooling, and greater pressure increases, although the differences were only statistically significant for the moistening (see also the subsection in section 3a). It is also consistent with Garcia-Carreras et al. (2013) who show that cold pools carry moisture northward into the Sahara from the Sahel during the premonsoon period.

Figures 5a and 5b show that colder cold pools give larger pressure increases, as expected. This relationship is most consistent for premonsoon cases, which have a correlation of 0.6 (statistically significant at $p < 0.11$), with monsoon and retreat periods having only weak correlations of 0.08 and -0.2 , respectively (not statistically significant). The overall correlation for the season was 0.3 (statistically significant at $p < 0.07$).

The overall distribution in Fig. 5a is similar to that shown in Fig. 5 of ESC08, except that a small percentage of cold pools in Engerer's study (1.5%) had either larger pressure increases or temperature deficits. Based on the total number of data points and the data points with temperature decrease greater than 14°C or pressure increase greater than 7 hPa in ESC08, we would expect approximately 0.6 data points with magnitudes of at least 14°C or 7 hPa for temperature decrease and pressure increase, respectively, to be found in our study if magnitudes of cold pool properties in Niamey were identical to those in Oklahoma. The fact that there were no such cold pools in our study, however, is not statistically significant at the 0.05 significance level to conclude that cold pools in Niamey are weaker in terms of temperature decrease and pressure increase when compared to Oklahoma. A considerably larger dataset would be needed to make any conclusions about the occurrence of such strong cold pools in Niamey when compared to Oklahoma. Note that MCSs tend to be observed at a particular point in their life cycle in Niamey. This was often either in a mature or dissipating stage, although difficult to differentiate at times due to only one radar data source and attenuation by rainfall as already discussed. Hence, stronger cold pools may be observed elsewhere in West Africa. This is a limitation of this

observational study, which was, by necessity, confined to one spatial point.

Observed nighttime cold pools are generally associated with higher values of pressure increase for a given temperature decrease than daytime ones (Fig. 5b). The reason for this is likely the fact that at night the boundary layer tends to be stable due to nocturnal cooling and during the day the surface layer is unstable. The magnitude of the cold pool-related change in temperature aloft is, therefore, greater than observed at the surface at night, and less during the day (Davies et al. 2005). The cold pool may also slide on top of the stably stratified surface layer at night (Heinold et al. 2013; Marsham et al. 2011a), significantly reducing the temperature decrease measured at the surface. However, both small and large decreases in surface temperature in Fig. 5b show that at least some of downdrafts at Niamey routinely reach the surface despite the presence of a nocturnal inversion. Figure 5b shows that pressure increases greater than ~ 5 hPa occurred only at night or in the morning (before 0800 LT), which is consistent with ESC08 and likely the result of deeper cold pools associated with maturing/dissipating MCSs and the known tendency for large organized systems at night over Niamey (Rickenbach et al. 2009).

ROLE OF MIDDLELEVEL DRYNESS

It was hypothesized that the stronger cold pools in the premonsoon period (with greater wind gusts, see section 3b) may be caused by seasonally drier midlevels in that period (Marsham et al. 2008; Barnes and Sieckman 1984). We test this hypothesis using a one-dimensional conceptual model, where radiosonde data were used to quantify midlevel dryness for each cold pool using θ_w (wet-bulb potential temperature) depression (i.e., difference between θ and θ_w , averaged between 550 and 750 hPa) using the nearest prestorm sounding. These soundings were between 38 min and 5 h, 52 min before the cold pool crossing. Despite the long gaps between the radio sounding and the cold pool in some cases, these were the best midlevel data available. In reality, the applicability of the one-dimensional model may be limited by significant horizontal gradients and transports; this may in future be tested in high-resolution modeling studies.

Figure 6 shows how close observed cold pool temperatures are to idealized descents of midlevel air. In this figure, we plot the departure from moist adiabats (DMA), defined as

$$\text{DMA} = \theta_{\text{cold pool}} - \text{mean}[\theta_{w(550-750 \text{ hPa})}].$$

Against midlevel dryness defined using the difference between mean potential temperature and wet-bulb

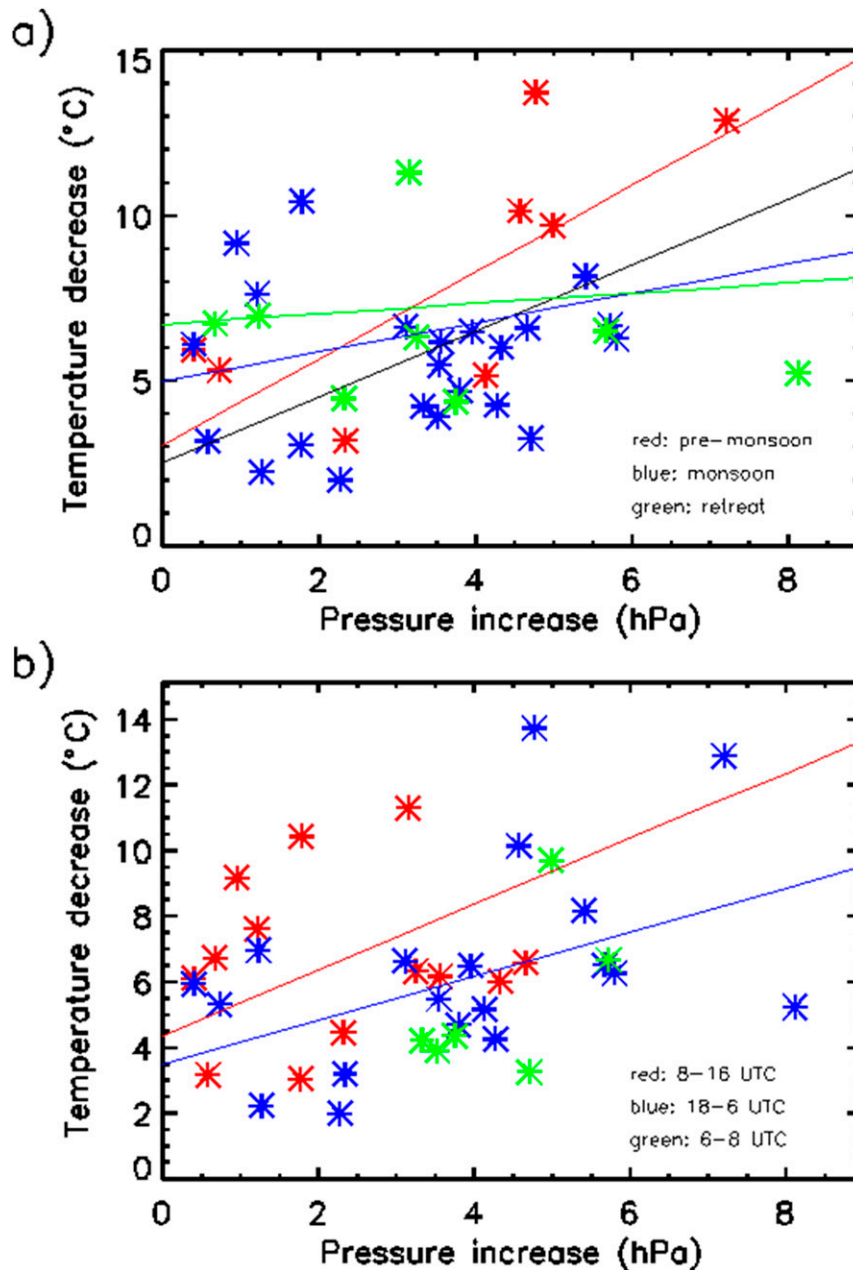


FIG. 5. Pressure increases and temperature decreases from cold pools. (a) Coloring represents the whole period and subperiods as in Fig. 3. (b) Coloring represents the time of day (red: 0800–1600 UTC, blue: 1800–0600 UTC, green: 0600–0800 UTC, there were no events between 1600 and 1800 UTC).

potential temperature in the 550–750-hPa layer. Therefore, Fig. 6 shows how the cold pool potential temperature minus the wet-bulb potential temperature of midlevels (y axis) depends on the midlevel θ_w depression. If midlevel air was cooled by evaporation of precipitation and descended while being kept saturated by continued evaporation then the air would descend moist adiabatically and the cold pool potential

temperature would equal the midlevel θ_w (y -axis value equals zero in Fig. 6). In contrast, if midlevel air instead descended completely dry adiabatically then the potential temperature of the cold pool would equal the potential temperature of the midlevels and data would lie on the one-to-one line in Fig. 6. Therefore, how far the data are from the one-to-one toward the x -axis line in Fig. 6 is a measure of the degree of saturation in the

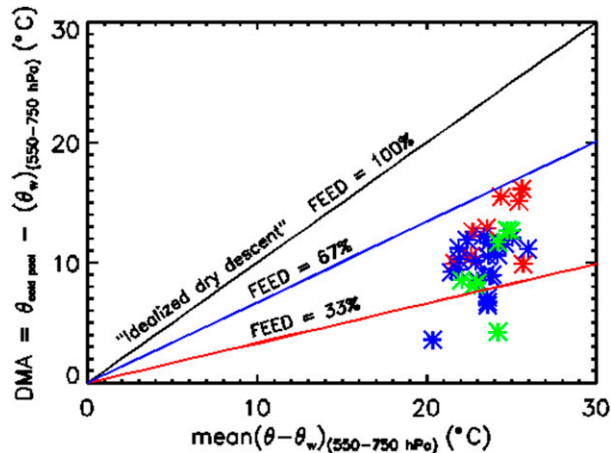


FIG. 6. Departure from moist adiabat (DMA), which equals $\{\theta_{\text{cold pool}} - \text{mean}[\theta_{w(550-750 \text{ hPa})}]\}$ vs midlevel dryness defined using the difference between mean $[\theta_{(550-750 \text{ hPa})}]$ and mean $[\theta_{w(550-750 \text{ hPa})}]$. Coloring of points represents the subperiods as in Fig. 3. Diagonal lines represent constant fractional evaporational energy deficit (FEED) of 100% (black), 67% (blue), and 33% (red).

idealized one-dimensional descent. We, therefore, refer to the y axis as the DMA and the ratio of both axes as the fractional evaporational energy deficit (FEED), with the one-to-one line of FEED = 100%.

The values in Fig. 6 can also be related to the energetics of the downdraft. For a fixed pressure of source air, the potential energy of cooling by evaporation is approximately proportional to the x-axis value (the energy is proportional to the tephigram area bounded by the θ_w line of saturated descending air and the theta line for unsaturated descending air, and here we approximate this by a triangle). As noted above, if FEED is zero, then the downdraft is fully saturated in its descent, and we could regard the downdraft convective available potential energy (DCAPE) to be a good measure of the downdraft potential energy released.

Figure 6 shows that $\theta_{\text{cold pool}}$ values are never equal to midlevel θ_w values, with the moistest cold pool having DMA of 3.6°C, confirming that no cold pool in our study was formed by the theoretical, perfectly moist adiabatic descent of midlevel air. In contrast, the highest value of DMA is 16.1°C. All data points lie below the line of FEED of 67% and the lowest data point has a FEED of 17.6%. The overall relationship suggests that drier midlevels are related to greater DMA and FEED (correlation between DMA and midlevel θ_w depression is 0.5 with $p < 0.001$, correlation between FEED and midlevel θ_w depression is 0.03 with $p < 0.89$). This suggests that the ability of precipitation to keep the descending parcel saturated decreases with drier midlevels, which may be due to greater mixing of dry air or

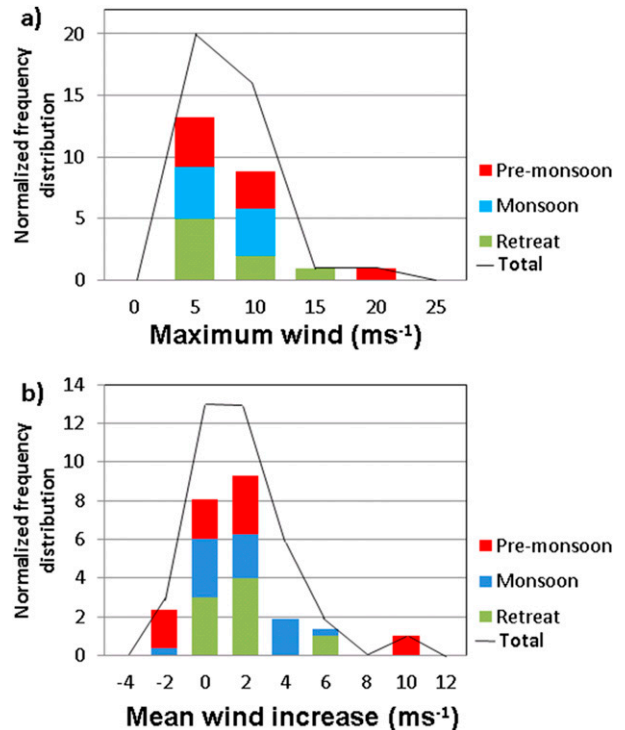


FIG. 7. As in Fig. 4, but for (a) 10-m wind gusts and (b) mean wind increases.

insufficient availability of precipitation to be evaporated into the descending parcel. Premonsoon data points have generally greater percentages of FEED and lie closer to the FEED of 67% line. This is not statistically significant, but suggests that the drier atmosphere in the premonsoon period may lead to drier descents.

b. Cold pool winds

The observed maximum wind gusts range from 4 to 22 m s^{-1} with most cold pools having gusts between 2.5 and 12.5 m s^{-1} (Fig. 7a). The mean wind can either increase (26 cases) or decrease (11 cases) during a cold pool passage, with the magnitudes of increase generally between 0 and 6 m s^{-1} , with the greatest value of increase being $\sim 10 \text{ m s}^{-1}$ (Fig. 7b). The magnitudes of the decreases were less than 3 m s^{-1} and were always associated with a mean decrease of the general environmental wind speed.

The mean for maximum wind gusts in the premonsoon period was 10.1 m s^{-1} , which was greater than that in the monsoon and retreat periods (7.6 and 7.5 m s^{-1} , respectively). This difference was, however, not statistically significant. There were comparable mean wind speed changes (+1.4, +1.6, and +1.4 for premonsoon, monsoon, and retreat, respectively). The mean premonsoon gusts were strongly affected by a single strong event on 17 June, when the highest gust of 21.4 m s^{-1} was

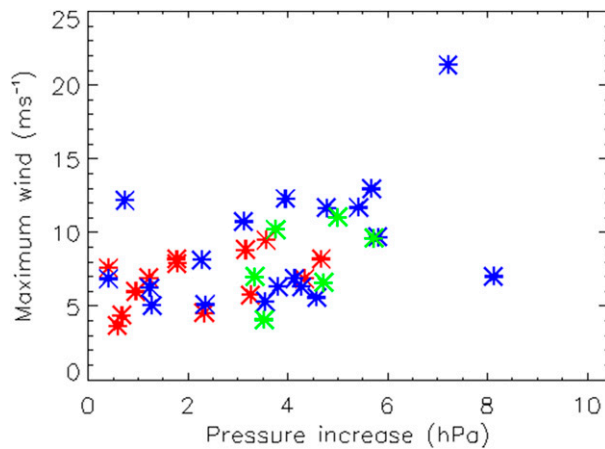


FIG. 8. Cold pool pressure increases and maximum wind gusts. Colors represent different times of day (red: 0800–1700 UTC, blue: 1900–0600 UTC, green: 0600–0800 UTC, no cold pool crossed between 1700 and 1900 UTC).

recorded. If this case was removed then the mean premonsoon gust decreased to 8.5 m s^{-1} (still higher than other subperiods, but again not significantly).

The relation between pressure changes and maximum wind gusts, which are partly driven by the pressure changes, has a correlation of 0.46 ($p < 0.004$, statistically significant) (Fig. 8). There was one outlier (the 17 June event), where additional features such as mixing of momentum from upper levels may have caused stronger winds than would be expected from the observed pressure increase alone. If this outlier is taken away, the correlation reduces to 0.42 ($p < 0.01$, still statistically significant). The diurnal distribution of cold pool-related wind gusts shows that the higher cold pool-related gusts (above $\sim 10 \text{ m s}^{-1}$) were not limited to the daytime. This contradicts the fact that the stably stratified nocturnal boundary layer can inhibit cold pool winds at night (Parker 2008; Marsham et al. 2011a); cold pools over Niamey from some of the mature nocturnal MCSs can clearly mix down through this nighttime stable layer (see also temperature changes in section 3a).

4. Conclusions

MCSs are an important feature of the West African monsoon, providing most of the rainfall over the Sahel. Cold pools contribute to the organization of these MCSs, form a crucial component of the monsoon flow (Marsham et al. 2013a), and ventilate the Saharan heat low (Garcia-Carreras et al. 2013). This study has quantified properties of cold pools from MCSs observed over Niamey in the Sahel during the 2006 AMMA field campaign, using a methodology similar to ESC08.

Every observed cold pool in this study was associated with a temperature decrease, ranging from 1.8° to 13.6°C , and a pressure increase, ranging from 0.4 to 8.1 hPa. These observed ranges generally agree with those observed by ESC08 in the United States, but are missing ESC08's largest values. Given the much smaller sample size of our study, it is not possible to say whether these more intense events are rarer in Niamey than the United States or whether our sample is too small to observe them.

The water vapor mixing ratio was found to decrease just after the cold pool passage in all but nine cases. The magnitude of the decrease did not exceed 3.4 g kg^{-1} . This initial decrease was in many cases followed by an increase in the mixing ratio of around 0.5 g kg^{-1} , sometimes to values greater than before the cold pool passage, which appears to be generated by the MCS rainfall. The mean equivalent potential temperature was found to increase in 6 out of the 38 cases, but decrease in others. A maximum in observed winds has been identified with every passage of an MCS, ranging from 3.7 to 21.6 m s^{-1} . The time-averaged 10-m mean wind from before to after the gust front was found to usually increase, although decreases were observed, with changes ranging from -2.3 to $+10.0 \text{ m s}^{-1}$.

Cold pools in the premonsoon period gave larger pressure increases and temperature decreases, as well as larger maximum wind gusts and mean wind increases, when compared to the monsoon and retreat periods. These were, however, not statistically significant. Premonsoon cold pools increased rather than decreased WVMR. Premonsoon cases gave little overall change in equivalent potential temperature, which tended to be decreased by cold pools in the monsoon and retreat periods. These differences in changes in WVMR and θ_e between cold pools during the premonsoon and later periods were statistically significant at the 90% significance level. Furthermore, we define the departure from moist adiabat (DMA) and fractional evaporational energy deficit (FEED) and use a simple 1D model to quantify how close the observed cold pools were near wet adiabatic (FEED = 0%) or dry adiabatic (FEED = 100%) descent. FEED varied from 17.6% to 64.5%, with drier descents for drier midlevels and during the premonsoon period (with only a correlation of 0.5 between DMA and midlevel θ_w depression). The importance of cold pools in the Sahel suggests that future studies should use AMMA observations to evaluate modeled cold pools in operational and research models. Such evaluations could make use of DMA and FEED as defined here, which would be strengthened by trajectory analyses from a high-resolution model.

The results show that early season cold pools provide high equivalent potential temperature air at low levels, which especially if reheated could feed later convection, once the high CIN is overcome (see also Torri et al. 2015). Later in the season, the cold pools reduce equivalent potential temperature but will still favor convection by lifting. The results are consistent with observations from Garcia-Carreras et al. (2013), who show that cold pools bring moist air toward the Saharan heat low early in the season. The results support the hypothesis that early in the monsoon season, when midlevels are drier and there is, therefore, greater diabatic cooling, cold pools will make a greater contribution to the monsoon flow (Marshall et al. 2013a).

Acknowledgments. We thank all the reviewers for their constructive and helpful comments. Surface meteorological data were obtained from the ARM Climate Research Facility (U.S. Department of Energy) deployed in Niamey in the AMMA campaign. Based on a French initiative, AMMA (<http://www.amma-international.org>) was built by an international group. MIT radar was made available to AMMA from Massachusetts Institute of Technology. AMMA-UK has been funded by NERC Grants NE/B505538/1 and NE/G018499/1. Thanks to Richard Pope and many others for practical help with using data analysis software.

REFERENCES

- American Meteorological Society, 2015: Mesoscale convective system. Glossary of Meteorology. [Available online at http://glossary.ametsoc.org/wiki/Mesoscale_convective_systems.]
- Aspliden, C. I., 1976: A classification of the structure of the tropical atmosphere and related energy fluxes. *J. Appl. Meteor.*, **15**, 692–697, doi:10.1175/1520-0450(1976)015<0692:ACOTSO>2.0.CO;2.
- Barnes, G. M., and K. Sieckman, 1984: The environment of fast-moving and slow-moving tropical mesoscale convective cloud lines. *Mon. Wea. Rev.*, **112**, 1782–1794, doi:10.1175/1520-0493(1984)112<1782:TEOFAS>2.0.CO;2.
- Birch, C. E., D. J. Parker, A. O’Leary, C. M. Taylor, J. H. Marshall, P. Harris, and G. Lister, 2013: The impact of soil moisture and atmospheric waves on the development of a mesoscale convective system: A model study of an observed AMMA case. *Quart. J. Roy. Meteor. Soc.*, **139**, 1712–1730, doi:10.1002/qj.2062.
- Charba, J., 1974: Application of gravity current model to analysis of squall-line gust front. *Mon. Wea. Rev.*, **102**, 140–156, doi:10.1175/1520-0493(1974)102<0140:AOGCMT>2.0.CO;2.
- Chong, M., 2010: The 11 August 2006 squall-line system as observed from MIT Doppler radar during the AMMA SOP. *Quart. J. Roy. Meteor. Soc.*, **136**, 209–226, doi:10.1002/qj.466.
- , P. Amayenc, G. Scialom, and J. Testud, 1987: A tropical squall line observed during the COPT 81 experiment in West Africa. Part I: Kinematic structure inferred from dual-Doppler radar data. *Mon. Wea. Rev.*, **115**, 670–694, doi:10.1175/1520-0493(1987)115<0670:ATSL0D>2.0.CO;2.
- Cram, J. M., R. A. Pielke, and W. R. Cotton, 1992: Numerical simulation and analysis of a prefrontal squall line. Part II: Propagation of the squall line as an internal gravity wave. *J. Atmos. Sci.*, **49**, 209–225, doi:10.1175/1520-0469(1992)049<0209:NSAAOA>2.0.CO;2.
- Davies, T., M. J. P. Cullen, A. J. Malcolm, M. H. Mawson, A. Staniforth, A. A. White, and N. Wood, 2005: A new dynamical core for the Met Office’s global and regional modelling of the atmosphere. *Quart. J. Roy. Meteor. Soc.*, **131**, 1759–1782, doi:10.1256/qj.04.101.
- Dhonneur, G., 1973: Study of a line squall in Niger Bend. *Bull. Amer. Meteor. Soc.*, **54**, 1075–1075.
- Dione, C., M. Lothon, D. Badiane, B. Campistron, F. Couvreux, F. Guichard, and S. Salle, 2014: Phenomenology of Sahelian convection observed in Niamey during the early monsoon. *Quart. J. Roy. Meteor. Soc.*, **140**, 500–516, doi:10.1002/qj.2149.
- Engerer, N. A., D. J. Stensrud, and M. C. Coniglio, 2008: Surface characteristics of observed cold pools. *Mon. Wea. Rev.*, **136**, 4839–4849, doi:10.1175/2008MWR2528.1.
- Flamant, C., J. P. Chaboureaud, D. J. Parker, C. A. Taylor, J. P. Cammas, O. Bock, and J. Pelon, 2007: Airborne observations of the impact of a convective system on the planetary boundary layer thermodynamics and aerosol distribution in the inter-tropical discontinuity region of the West African Monsoon. *Quart. J. Roy. Meteor. Soc.*, **133**, 1175–1189, doi:10.1002/qj.97.
- Fortune, M., 1980: Properties of African squall lines inferred from time-lapse satellite imagery. *Mon. Wea. Rev.*, **108**, 153–168, doi:10.1175/1520-0493(1980)108<0153:POASLI>2.0.CO;2.
- Fovell, R. G., and Y. Ogura, 1989: Effect of vertical wind shear on numerically simulated multicell storm structure. *J. Atmos. Sci.*, **46**, 3144–3176, doi:10.1175/1520-0469(1989)046<3144:EOVWSO>2.0.CO;2.
- Fujita, T., 1963: Precise reduction of radiation data from meteorological satellites. *J. Opt. Soc. Amer.*, **53**, 1331.
- Futyan, J. M., and A. D. Del Genio, 2007: Deep convective system evolution over Africa and the tropical Atlantic. *J. Climate*, **20**, 5041–5060, doi:10.1175/JCLI4297.1.
- Garcia-Carreras, L., and Coauthors, 2013: The impact of convective cold pool outflows on model biases in the Sahara. *Geophys. Res. Lett.*, **40**, 1647–1652, doi:10.1002/grl.50239.
- Hamilton, R. A., J. W. Archbold, and C. K. M. Douglas, 1945: Meteorology of Nigeria and adjacent territory. *Quart. J. Roy. Meteor. Soc.*, **71**, 231–264, doi:10.1002/qj.49707130905.
- Heinold, B., P. Knippertz, J. H. Marshall, S. Fiedler, N. S. Dixon, K. Schepanski, B. Laurent, and I. Tegen, 2013: The role of deep convection and nocturnal low-level jets for dust emission in summertime West Africa: Estimates from convection-permitting simulations. *J. Geophys. Res. Atmos.*, **118**, 4385–4400, doi:10.1002/jgrd.50402.
- Holdridge, D., J. Kyrouac, and R. Coulter, 2013a: Surface Meteorological Instrumentation (NIMMET), 2006-06-01 to 2006-09-30, 13.4773°N, 2.1758°E, ARM Mobile Facility (NIM) Niamey, Niger (M1). Updated daily, ARM Climate Research Facility, accessed 15 July 2013. [Available online at <http://www.arm.gov/sites/amf/nim/>.]
- , —, and —, 2013b: Balloon-Borne Sounding System (SONDEWNP), 2006-06-01 to 2006-09-30, 13.4773°N, 2.1758°E, ARM Mobile Facility (NIM) Niamey, Niger (M1). Updated daily, ARM Climate Research Facility, accessed 15 July 2013, doi:10.5439/1021460.
- Lebel, T., and L. LeBarbe, 1997: Rainfall monitoring during HAPEX-Sahel. 2. Point and areal estimation at the event and seasonal scales. *J. Hydrol.*, **188–189**, 97–122, doi:10.1016/S0022-1694(96)03325-2.

- , J. D. Taupin, and N. D'Amato, 1997: Rainfall monitoring during HAPEX-Sahel. 1. General rainfall conditions and climatology. *J. Hydrol.*, **188–189**, 74–96, doi:[10.1016/S0022-1694\(96\)03155-1](https://doi.org/10.1016/S0022-1694(96)03155-1).
- Lothon, M., B. Campistron, M. Chong, F. Couvreur, F. Guichard, C. Rio, and E. Williams, 2011: Life cycle of a mesoscale circular gust front observed by a C-band Doppler radar in West Africa. *Mon. Wea. Rev.*, **139**, 1370–1388, doi:[10.1175/2010MWR3480.1](https://doi.org/10.1175/2010MWR3480.1).
- Marshall, J. H., D. J. Parker, C. M. Grams, C. M. Taylor, and J. M. Haywood, 2008: Uplift of Saharan dust south of the intertropical discontinuity. *J. Geophys. Res.*, **113**, D21102, doi:[10.1029/2008JD009844](https://doi.org/10.1029/2008JD009844).
- , S. B. Trier, T. M. Weckwerth, and J. W. Wilson, 2011a: Observations of elevated convection initiation leading to a surface-based squall line during 13 June IHOP_2002. *Mon. Wea. Rev.*, **139**, 247–271, doi:[10.1175/2010MWR3422.1](https://doi.org/10.1175/2010MWR3422.1).
- , P. Knippertz, N. S. Dixon, D. J. Parker, and G. M. S. Lister, 2011b: The importance of the representation of deep convection for modeled dust-generating winds over West Africa during summer. *Geophys. Res. Lett.*, **38**, L16803, doi:[10.1029/2011GL048368](https://doi.org/10.1029/2011GL048368).
- , N. S. Dixon, L. Garcia-Carreras, G. M. S. Lister, D. J. Parker, P. Knippertz, and C. E. Birch, 2013a: The role of moist convection in the West African monsoon system: Insights from continental-scale convection-permitting simulations. *Geophys. Res. Lett.*, **40**, 1843–1849, doi:[10.1002/grl.50347](https://doi.org/10.1002/grl.50347).
- , M. Hobby, C. J. T. Allen, J. R. Banks, M. Bart, B. J. Brooks, and R. Washington, 2013b: Meteorology and dust in the central Sahara: Observations from Fennec supersite-1 during the June 2011 Intensive Observation Period. *J. Geophys. Res. Atmos.*, **118**, 4069–4089, doi:[10.1002/jgrd.50211](https://doi.org/10.1002/jgrd.50211).
- Mathon, V., H. Laurent, and T. Lebel, 2002: Mesoscale convective system rainfall in the Sahel. *J. Appl. Meteor.*, **41**, 1081–1092, doi:[10.1175/1520-0450\(2002\)041<1081:MCSRIT>2.0.CO;2](https://doi.org/10.1175/1520-0450(2002)041<1081:MCSRIT>2.0.CO;2).
- McGraw-Herdeg, M., 2010: Dusty gust fronts and their contributions to long-lived convection in West Africa. Ph.D. thesis, Department of Electrical Engineering and Computer Science, 157 pp.
- Mueller, C. K., and R. E. Carbone, 1987: Dynamics of a thunderstorm outflow. *J. Atmos. Sci.*, **44**, 1879–1898, doi:[10.1175/1520-0469\(1987\)044<1879:DOATO>2.0.CO;2](https://doi.org/10.1175/1520-0469(1987)044<1879:DOATO>2.0.CO;2).
- Parker, D. J., C. D. Thorncroft, R. R. Burton, and A. Diongue-Niang, 2005: Analysis of the African easterly jet, using aircraft observations from the JET2000 experiment. *Quart. J. Roy. Meteor. Soc.*, **131**, 1461–1482, doi:[10.1256/qj.03.189](https://doi.org/10.1256/qj.03.189).
- Parker, M. D., 2008: Response of simulated squall lines to low-level cooling. *J. Atmos. Sci.*, **65**, 1323–1341, doi:[10.1175/2007JAS2507.1](https://doi.org/10.1175/2007JAS2507.1).
- , and R. H. Johnson, 2004a: Simulated convective lines with leading precipitation. Part I: Governing dynamics. *J. Atmos. Sci.*, **61**, 1637–1655, doi:[10.1175/1520-0469\(2004\)061<1637:SCLWLP>2.0.CO;2](https://doi.org/10.1175/1520-0469(2004)061<1637:SCLWLP>2.0.CO;2).
- , and —, 2004b: Simulated convective lines with leading precipitation. Part II: Evolution and maintenance. *J. Atmos. Sci.*, **61**, 1656–1673, doi:[10.1175/1520-0469\(2004\)061<1656:SCLWLP>2.0.CO;2](https://doi.org/10.1175/1520-0469(2004)061<1656:SCLWLP>2.0.CO;2).
- Redelsperger, J.-L., and J. P. Lafore, 1988: A three-dimensional simulation of a tropical squall line: Convective organization and thermodynamic vertical transport. *J. Atmos. Sci.*, **45**, 1334–1356, doi:[10.1175/1520-0469\(1988\)045<1334:ATDSOA>2.0.CO;2](https://doi.org/10.1175/1520-0469(1988)045<1334:ATDSOA>2.0.CO;2).
- , C. D. Thorncroft, A. Diedhiou, T. Lebel, D. J. Parker, and J. Polcher, 2006: African Monsoon Multidisciplinary Analysis: An international research project and field campaign. *Bull. Amer. Meteor. Soc.*, **87**, 1739–1746, doi:[10.1175/BAMS-87-12-1739](https://doi.org/10.1175/BAMS-87-12-1739).
- Rickenbach, T., R. N. Ferreira, N. Guy, and E. Williams, 2009: Radar-observed squall line propagation and the diurnal cycle of convection in Niamey, Niger, during the 2006 African Monsoon and Multidisciplinary Analyses Intensive Observing Period. *J. Geophys. Res.*, **114**, D03107, doi:[10.1029/2008JD010871](https://doi.org/10.1029/2008JD010871).
- Roca, R., S. Louvet, L. Picon, and M. Desbois, 2005: A study of convective systems, water vapour and top of the atmosphere cloud radiative forcing over the Indian Ocean using INSAT-1B and ERBE data. *Meteor. Atmos. Phys.*, **90**, 49–65, doi:[10.1007/s00703-004-0098-3](https://doi.org/10.1007/s00703-004-0098-3).
- Rotunno, R., J. B. Klemp, and M. L. Weisman, 1988: A theory for strong, long-lived squall lines. *J. Atmos. Sci.*, **45**, 463–485, doi:[10.1175/1520-0469\(1988\)045<0463:ATFSL>2.0.CO;2](https://doi.org/10.1175/1520-0469(1988)045<0463:ATFSL>2.0.CO;2).
- Szeto, K. K., and H. R. Cho, 1994a: A numerical investigation of squall lines. Part I: The control experiment. *J. Atmos. Sci.*, **51**, 414–424, doi:[10.1175/1520-0469\(1994\)051<0414:ANIOSL>2.0.CO;2](https://doi.org/10.1175/1520-0469(1994)051<0414:ANIOSL>2.0.CO;2).
- , and —, 1994b: A numerical investigation of squall lines. Part II: The mechanics of evolution. *J. Atmos. Sci.*, **51**, 425–433, doi:[10.1175/1520-0469\(1994\)051<0425:ANIOSL>2.0.CO;2](https://doi.org/10.1175/1520-0469(1994)051<0425:ANIOSL>2.0.CO;2).
- Thorpe, A. J., M. J. Miller, and M. W. Moncrieff, 1982: Two-dimensional convection in non-constant shear—A model of mid-latitude squall lines. *Quart. J. Roy. Meteor. Soc.*, **108**, 739–762, doi:[10.1002/qj.49710845802](https://doi.org/10.1002/qj.49710845802).
- Torri, G., Z. Kuang, and Y. Tian, 2015: Mechanisms for convection triggering by cold pools. *Geophys. Res. Lett.*, **42**, 1943–1950, doi:[10.1002/2015GL063227](https://doi.org/10.1002/2015GL063227).
- Tratt, D. M., M. H. Hecht, D. C. Catling, E. C. Samulon, and P. H. Smith, 2003: In situ measurement of dust devil dynamics: Toward a strategy for Mars. *J. Geophys. Res.*, **108**, 5116, doi:[10.1029/2003JE002161](https://doi.org/10.1029/2003JE002161).
- Trier, S. B., W. C. Skamarock, and M. A. LeMone, 1997: Structure and evolution of the 22 February 1993 TOGA COARE squall line: Organization mechanisms inferred from numerical simulation. *J. Atmos. Sci.*, **54**, 386–407, doi:[10.1175/1520-0469\(1997\)054<0386:SAEOTF>2.0.CO;2](https://doi.org/10.1175/1520-0469(1997)054<0386:SAEOTF>2.0.CO;2).
- Weisman, M. L., J. B. Klemp, and R. Rotunno, 1988: Structure and evolution of numerically simulated squall lines. *J. Atmos. Sci.*, **45**, 1990–2013, doi:[10.1175/1520-0469\(1988\)045<1990:SAEONS>2.0.CO;2](https://doi.org/10.1175/1520-0469(1988)045<1990:SAEONS>2.0.CO;2).